Stanford Exploration Project, Report 111, June 9, 2002, pages 239–253

Finite-difference ω-x migration of unregularized seismic data

Ioan Vlad[1]

ABSTRACT

Wavefield downward continuation does not need to be done on a structured spatial mesh. Semistructured meshes have advantages (no need for regularization before migration) but they sometimes produce artifacts. There are at least two acquisition settings which will not result in artifacts. The implementation is simple. I present a 2D zero-offset ω-x semistructured mesh migration (SMM) of a synthetic dataset. Its outputs are compared with those of ω-x migration on a regular grid, with zero traces inserted in the place of missing data. There are several potential ways of removing the artifacts. Extension to 3D is also possible.

INTRODUCTION

Common sense and basic physics suggest that in order to continue a field (gravitational, magnetic, wavefield...) into a direction, it is necessary to know the values of the field on one or more surfaces nonparallel to the continuation direction, and the law that governs the field (approximations can be made or field laws inferred so that we need only one surface). Because field quantities are usually invariants, nothing mandates that field continuations be done on Cartesian grids (although in many cases it is numerically convenient to do so). In particular, a look at the 45° downward continuation equation (Claerbout, 1999) shows that it can be written as:

$$\frac{2i\omega}{v}\frac{\partial Q}{\partial z}+\left(1-\frac{v}{2i\omega}\frac{\partial}{\partial z}\right)\Delta Q=0 \tag{1}$$

where ΔQ, the Laplacian of Q, is an invariant. It can also be computed on an unstructured spatial mesh. In principle, this means that semistructured mesh migration (SMM) is feasible. I called the mesh semistructured because it is regular in time, but unstructured in space.

SMM ADVANTAGES AND DISADVANTAGES

There are several pros and cons about doing prestack SMM. First, let us examine the consequences of the assumption that SMM is feasible and accurate. The need for regularization

[1]**email:** nick@sep.stanford.edu

before or during migration would disappear. Regularization would be performed after migration when the imaging condition is applied and simplified, amounting to an image interpolation. Only raw, uninterpolated data would be fed into the migration process, leading to a more accurate image than that made from a regularized dataset consisting entirely of interpolated data. The need to fill in with large amounts of zero traces would disappear, leading to computational savings. Also, using the original acquisition geometry for imaging can be a step towards constructing a probability map of the seismic image: the extra incertitude introduced by interpolation before downward continuation is eliminated, and therefore is not propagated through hundreds of depth steps. Such goals are certainly desirable.

The main problem stems from computing the Laplacian on a grid that is too sparse in places (close to spatial aliasing) or whose step size varies too quickly. Previous attempts (Dellinger and Muir, 1986) as well as the results of this work show that abrupt variations in the mesh size lead to numerical artifacts under the form of reflections off the irregularities in the grid. Such spurious reflections do not appear when the mesh step varies smoothly, or when the variation is less than half the grid step size. Therefore, two straightforward SMM applications are:

1. Migrating reflection data acquired from a platform moving with a nonconstant velocity (i.e., seismic acquisition ship which was not able to maintain constant speed; GPR vehicle that had to accelerate or decelerate; radar-bearing aircraft that encounters various air currents). In all these cases, the velocity variation is small enough that it should lead to a smoothly-varying grid.

2. Migrating reflection data acquired on a *heated atomic lattice* – a regular grid whose nodes have been displaced with small (known) amounts from the periodic positions.

In neither of these cases was the data irregular enough to justify the cost of full-fledged regularization, which involves interpolating the whole dataset. Most often the fact that the mesh is not really regular is simply overlooked. Applying SMM to such datasets will surely increase the quality of the image. The implementation is simple, consisting (at least for the 2D zero-offset case that has been implemented, and for its prestack extension) of simply replacing the (1,-2,1) coefficients of the second derivative in the differencing star with sets of three precomputed geometry-dependent values.

COMPUTING DERIVATIVES ON A SEMISTRUCTURED MESH

Let $Q(\omega,x,z)$ denote a 2D zero-offset seismic wavefield, regularly sampled (and Fourier transformed) in time, but irregularly sampled in space. The measured surface dataset is $Q(\omega,x,z=0)$. For downward continuing Q with (1) we need to write differencing stars for $\frac{\partial Q}{\partial z}$ and for $\frac{\partial^2 Q}{\partial x^2}$. Fig. 1 shows the differencing star for the entire equation and defines shorthand notations. Since the differencing star spans only two values of z, it does not matter whether the sampling along the z axis is regular or not. I denote:

$$z_2 - z_1 = \delta z. \tag{2}$$

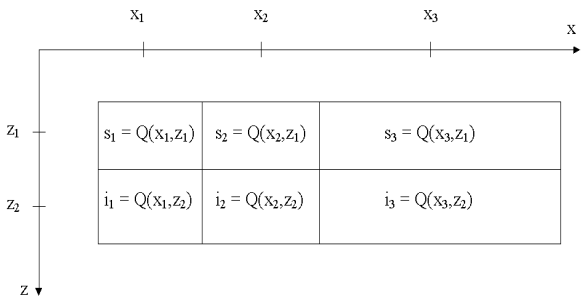

Figure 1: Differencing star for solving eq. 1 with the finite difference method; s_1, s_2, s_3, i_1, i_2, i_3 are just notations. This is the general case: the distance $x_2 - x_1$ is not necessarily equal to $x_3 - x_2$. nick1-diffstar [NR]

All derivatives will be considered to be computed in the middle of the differencing star. When $x_2 - x_1 = x_3 - x_2$, the middle is in x_2. When the two distances are drastically different, the middle is not in x_2 any more and errors are introduced. This may be the cause of the spurious reflections off the large variations in grid steps that are visible in the bottom panel of Fig. 4. Dellinger and Muir (1986) discuss this problem and suggest that letting the gridpoints drift across x as we downward continue can solve it. In order to examine the extent to which this problem affects the data, I will simply pretend that the problem does not exist, and observe its negative effects. So, given the values of a function $y(x)$ in three points, x_1, x_2 and x_3, with $x_1 < x_2 < x_3$, the second derivative can be computed by finding the coefficients of parabola that fits through the three points. The second derivative is twice the coefficient of the second-degree term in the parabola expression. Thus, by denoting:

$$k_i = \frac{1}{\prod_{j \in \Psi - \{i\}} (x_j - x_i)}, \quad i \in \Psi = \{1,2,3\}, \tag{3}$$

which can be more explicitly written out as

$$k_1 = \frac{1}{(x_3 - x_1)(x_2 - x_1)}, \tag{4}$$

$$k_2 = \frac{-1}{(x_3 - x_2)(x_2 - x_1)}, \tag{5}$$

$$k_3 = \frac{1}{(x_3 - x_1)(x_3 - x_2)}, \tag{6}$$

the second derivative is

$$\frac{d^2y}{dx^2} = 2(k_1 y_1 + k_2 y_2 + k_3 y_3). \tag{7}$$

The same formula is obtained by computing a first-order approximation of the second derivative as the first derivative of the first derivative in the point x_2. It should be noticed that the Laplacian is a low-pass filter of the original functionr. In other words, the curvature of the hyperbola is the same in each of the three points it fits through; $x_3 - x_2$ must be really different from $x_2 - x_1$ in order for the curvature-fitting hyperbola to be affected by the error

and for artifacts to be generated. This explains why the method is so robust. As Fig. 3 shows, artifacts start to become barely visible when $x_3 - x_2 = 2(x_2 - x_1)$. The partial derivatives in x of even order higher than two of the wavefield will be even more robust. A method that would make use not of the second-order derivatives but of the fourth-order ones, would be much less affected by the spurious reflections.

Using the notations in Fig. 1 and eq. (2), the second derivative expression in (7), and employing a Crank-Nicolson scheme to compute the second derivative in x, we obtain the following differencing stars:

$$\frac{\partial^2 Q}{\partial x^2} = k_1(i_1 + s_1) + k_2(i_2 + s_2) + k_3(i_3 + s_3), \tag{8}$$

$$\frac{\partial Q}{\partial z} = \frac{1}{\delta z}(i_2 - s_2), \tag{9}$$

$$\frac{\partial^3 Q}{\partial z \partial x^2} = \frac{2k_1}{\delta z}(i_1 - s_1) + \frac{2k_2}{\delta z}(i_2 - s_2) + \frac{2k_3}{\delta z}(i_3 - s_3). \tag{10}$$

The way the derivatives of a function are computed on a irregular mesh does not depend on the nature of the function, but the result of the computation does: the lower the frequency content, the better. This means that longer wavelengths will generate less artifacts, and the spatio-temporal frequency content of the spurious reflections will therefore be biased towards the high part of the spectrum. Practically no artifacts should be produced when the function has a very low frequency content, as is the case with potential fields. Upward or downward continuation of potential fields on a unstructured mesh should be very accurate.

IMPLEMENTATION OF A 2D, ZERO-OFFSET, CONSTANT-VELOCITY ω-X SMM

Although it is not easy to find irregularly sampled zero-offset non-synthetic reflection datasets, such a case was chosen for investigation because of its simplicity; any results should be directly applicable to the prestack case.

The Appendix shows a derivation for the 15° (parabolic) wave equation (38) and for the 45° one (37). Both can be expressed as:

$$a Q_{xxz} + Q_{xx} + b Q_z = 0, \tag{11}$$

where the subscripts denote partial derivatives along the corresponding axes. Plugging in the templates in (8), (9) (10), we get:

$$\begin{aligned} &\left(\tfrac{2ak_1}{\delta z} + k_1\right) i_1 + \left(\tfrac{2ak_2+b}{\delta z} + k_2\right) i_2 + \left(\tfrac{2ak_3}{\delta z} + k_3\right) i_3 = \\ &\left(\tfrac{2ak_1}{\delta z} - k_1\right) s_1 + \left(\tfrac{2ak_2+b}{\delta z} - k_2\right) s_2 + \left(\tfrac{2ak_3}{\delta z} - k_3\right) s_3. \end{aligned} \tag{12}$$

In the case of the 15° equation, $a = 0$, and for the 45° one, $a = \frac{iv}{2\omega}$. In both cases $b = \frac{2i\omega}{v}$. They are the same as for the regular sampling case, which is simply a particular case of this equation (with particular values of k_i). The stability of the downward continuation undertaken in this manner is proven for all practical purposes by the results in Figs. 3 and 4. This means that the special stability precautions taken by Dellinger and Muir (1986) are an unnecessary complication.

The resulting tridiagonal system is solved and the values of $Q(\omega, x, z_2)$ are found. The lens term (40) which is applied after each downward continuation step with the above described equations does not depend in any way on the sampling of the x-axis and is therefore the same as in ω - x migrations of evenly sampled data.

Unfortunately, the so-called 1/6 trick [Claerbout (1985b), section 4.3] cannot be straightforwardly applied when the spatial axis is unevenly sampled. With a bit of work, an equivalent formula can also be deduced for the irregular sampling case.

The proof in the Appendix ensures that no hidden regular sampling assumption has been incorporated in the 15° and 45° wave equation approximations.

SMM RESULTS - PRESENTATION AND DISCUSSION

I examined the SMM results on a simple synthetic dataset. I chose the one in Claerbout (1999) because it was small, simple, and the migration result was already known. First, I produced a surrogate irregular dataset - a zero offset section that was densely and regularly sampled across the x axis (see Fig. 2, upper panel). The image was migrated with the SMM code, as if it were a irregularly sampled dataset. Only the numerical values of the traces' coordinates were making it regular; the code was the same as for the truly irregular cases. The result is displayed in the middle panel of Fig. 2. The input data was "made" irregular by applying masks (shown in the bottom part of Fig. 2). SMM was performed on the traces present in the mask. For comparison, zero traces were introduced at the locations that were not present in the masks and surrogate irregular migration was performed.

Fig. 3 shows the input data (top panel), the zero-traces inserted migration (middle panel) and the SMM (bottom panel). The irregularity introduced by the mask is mild (the sixth trace has been eliminated in two regions). Inserting zero traces and imaging on a regular grid introduces noise farther away from the missing traces as depth increases. Overall, the image is full of incoherent high-frequency noise. Instead, the SMM result introduces no such problems. Even if the jump in sampling rate is large at the place of the missing traces (the step becomes $2 \cdot dx$ instead of dx), the reflections off the side of the grid are minor. This makes me believe that for jumps in the grid step of the order of half of dx and under, the artifacts would be negligible.

Fig. 4 shows the effect of severe irregularities. Both images are severely affected. The S/N ratio of the zero-traces inserted surrogate irregular migration result is lowered to the limit of interpretablity, and any mistake while interpolating the traces (if we interpolate instead of inserting zero traces) would probably have severe effects as well. The SMM result is plagued

by strong spurious reflections, but we notice that these are: a) localized, and b) highly coherent and dipping in the opposite direction from the true local dips. These are prone to filtering with a reasonable apriori assumption about the direction of the dip, and can be obtained as well from unmigrated data. The SMM image overall is crisp and interpretable. The fact that the incoherent noise has not been increased is particularly important because input datasets already suffer from a S/N problem, such as those in crustal seismology.

DEALING WITH THE SPURIOUS REFLECTIONS

There are five basic ways in which spurious reflections can be eliminated: 1) Letting the mesh points drift across the x axis as we downward continue. This approach, suggested by Dellinger and Muir (1986), would regularize the spatial grid and address the actual cause of the problem. 2) Planting interpolated traces at strategic locations. 3) Solving for a wave equation that incorporates the grid irregularity (dx as a function of x, or by applying a warping transform). 4) Filtering them out based on the fact that they are localized and highly coherent and their dip is opposite from that of local geologic dip. 5) Avoiding the problem altogether by using a numerical method for downward continuation that handles irregular data better than the finite difference method.

Method 1 seems to be the most elegant and efficient. For all methods, the biggest problem is posed by large gaps in the data coverage which would still need to be filled in with interpolated traces. A minimum trace density, related to the minimum spatial wavelength present in the data, must be maintained. The recent advances in interpolation methods of nonuniformly sampled data (Aldroubi and Grochenig, 2001) can be instrumental in this respect. Even with interpolation, the number of fill-in traces required will be smaller for an unconstrained mesh than that in the case of a Cartesian mesh. This is due to the Cartesian lattices not being the best at filling space; the same area can be covered by fewer traces placed on a quasi-regular triangular mesh. This at least should offset the burden of node number bookkeeping for an unstructured mesh. Large coverage gaps can be covered using the boundary element method. This method was created with the specific goal of not having to deal with very large numbers of elements inside a domain – its elements are only on the border of the domain. Another solution may be presented by the finite element method Marfurt (1984), which naturally handles unstructured meshes.

EXTENSION TO 3D

Because the Laplacian of a function is an invariant, the method should work the same way in 3D. Computing the Laplacian of a function of two arguments in the nodes of an unstructured mesh is an interesting mathematical problem. The simplest approach, analoguous to the one used for Cartesian grids, is to interpolate a surface through local sets of points and to compute the Laplacian analytically from its coefficients:

$$z = a + bx + cy + dx^2 + exy + fy^2 + gx^2y^2, \tag{13}$$

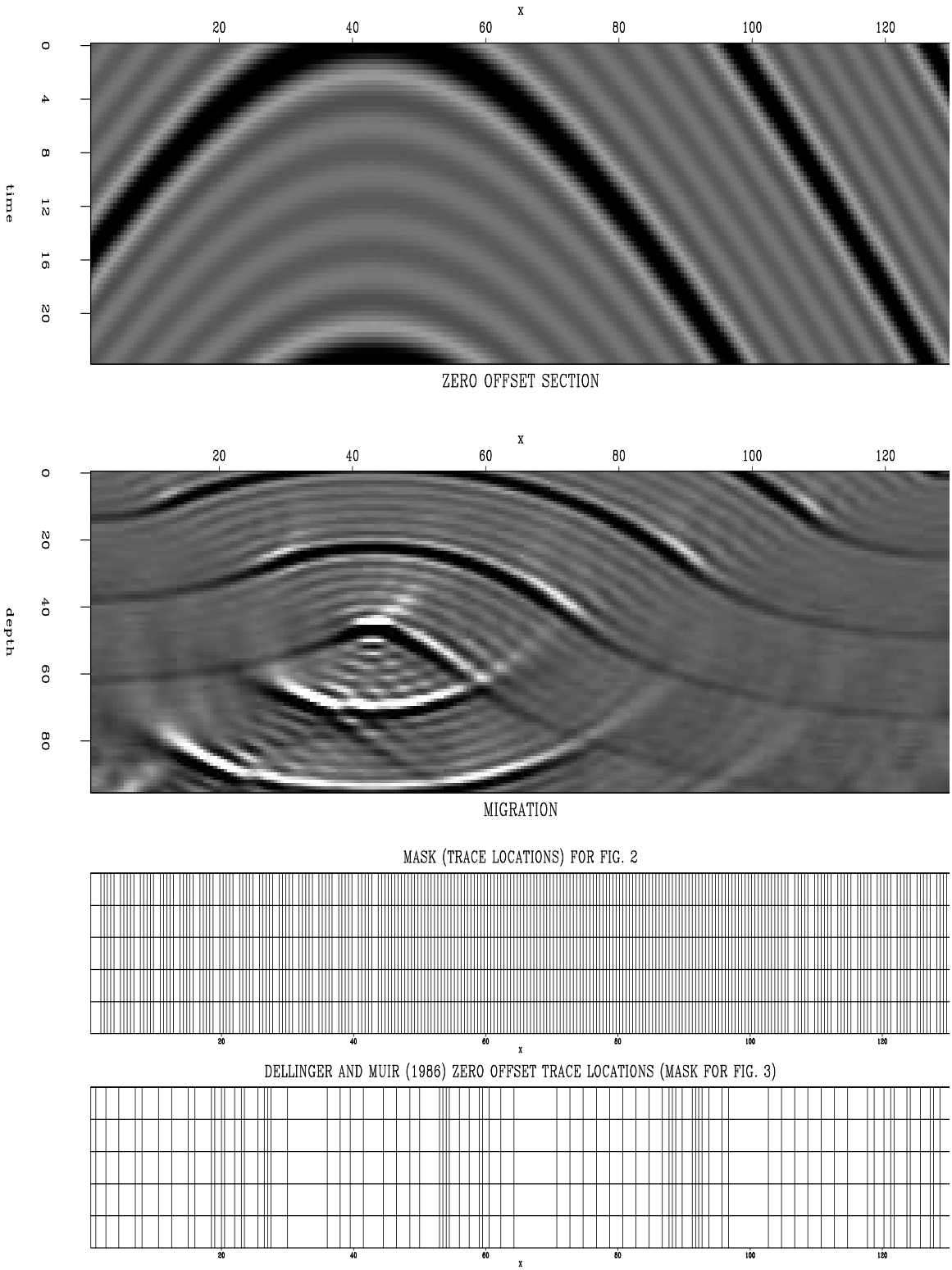

Figure 2: Input data from Claerbout (1999), its surrogate irregular 45° migration and the sampling masks used for creating irregularly sampled datasets nick1-init [ER]

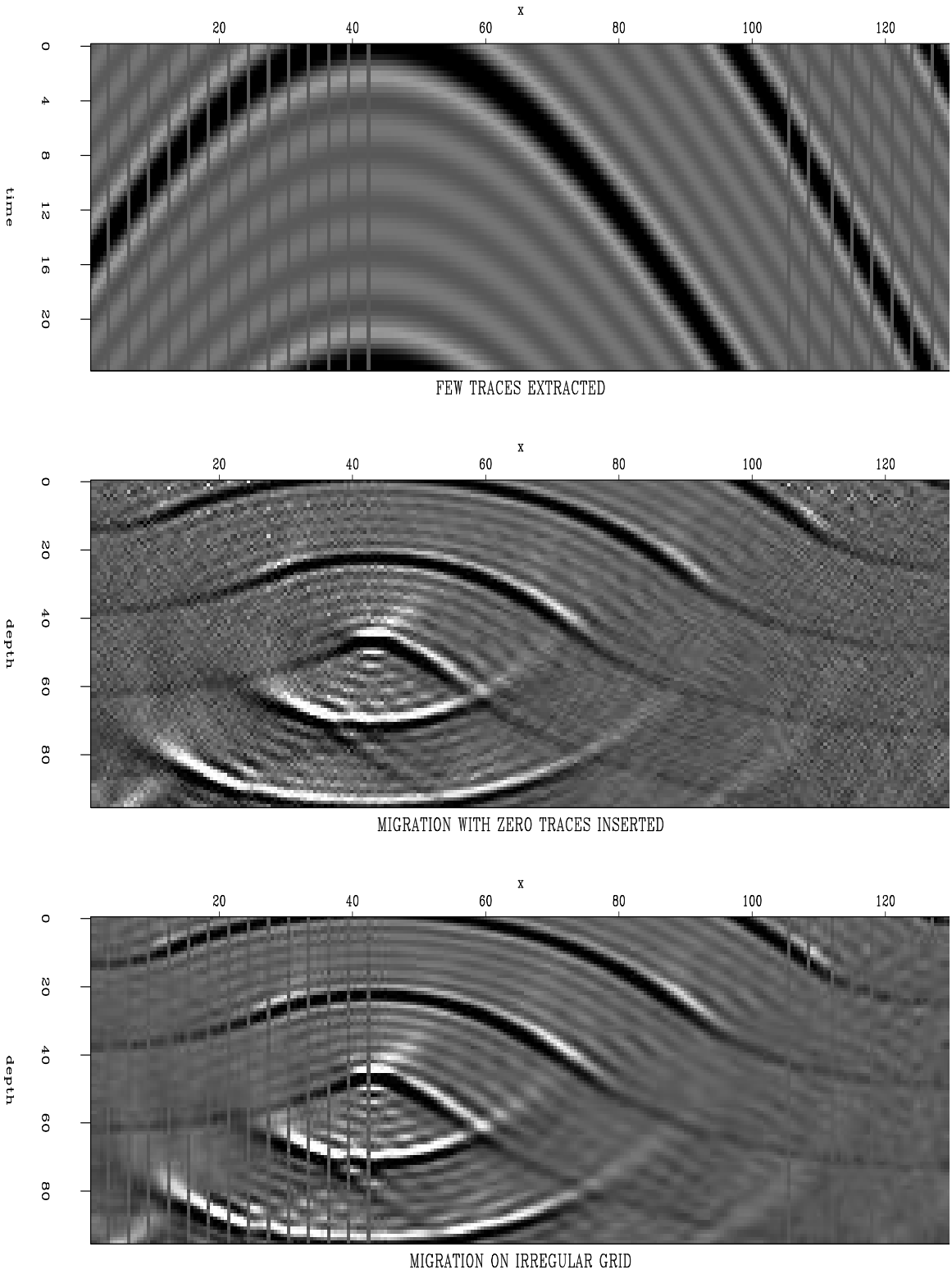

Figure 3: Input data (top panel), migration with zero-traces inserted (middle panel) and the SMM (bottom panel) nick1-midtk [ER]

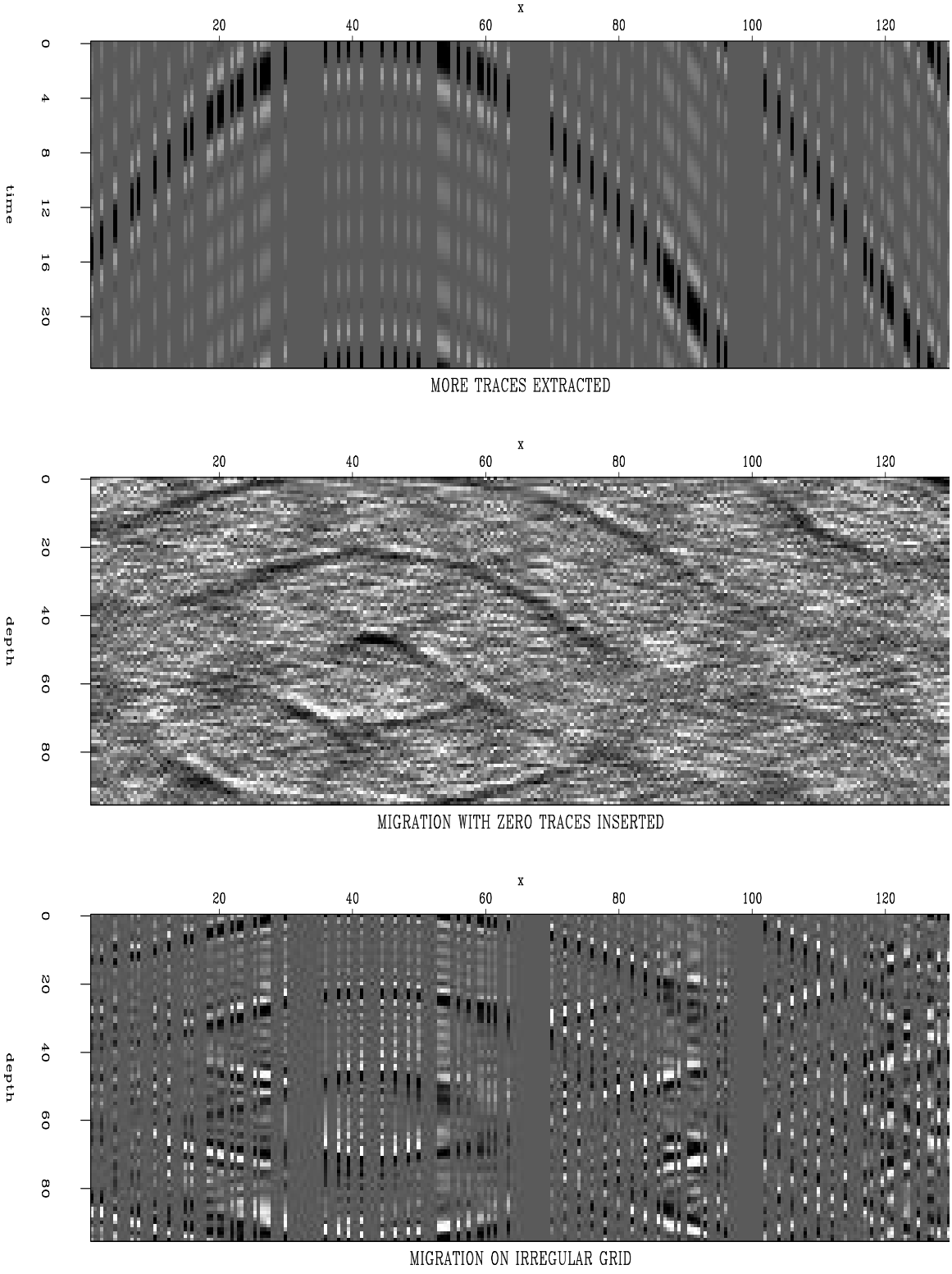

Figure 4: Input data (top panel), migration with zero-traces inserted (middle panel) and the SMM (bottom panel) nick1-reflgrid [ER]

$$\Delta z = 2d + 2f + 2g(x^2 + y^2). \tag{14}$$

Since the surface has seven terms, we must know the function $z = f(x,y)$ at seven points in order to find the Laplacian at one of the seven. This means solving a 7×7 linear system to find the coefficients a, b, c, d, e, f and g, given three pairs of (x,y,z) points. It seems frustrating that we have to compute all the seven coefficients while using only the values of d, f, and g. Fortunately, we do not have to solve innumerable amounts of 7×7 systems for each downward continuation step: the x and y values depend only on the geometry of the spatial mesh. For each point, the matrix inversion can be done only once: in the beginning, and after that for each point. We only need to multiply the vector of z values with three rows of the precomputed inverted matrix in order to find out the values of d, f, and g.

On a Cartesian grid, only five values are needed to compute the Laplacian. In that case, we also deal with two extra "hidden" relationships that state the particular geometrical relationships between the five points. In the general case, we do not have that information and, therefore, need more points.

The Laplacian may be found in other ways as well; perhaps interpolating with splines or other basis functions the entire wavefield - not just local neighbourhoods - at each depth step. The fastest and most elegant approach would nevertheless not involve finding a complete analytical expression of the wavefield function, but only its curvature information represented by the Laplacian.

CONCLUSIONS

2D SMM implementation is simple – just replace the (1,-2,1) Laplacian coefficients in the differencing star with precomputed sets of geometry-dependent coefficients. It is also numerically stable. The images produced are clear and crisp, the only artifacts being the spurious reflections off the abrupt variations in grid size. There are several possible ways of eliminating them. These artifacts are not likely to be generated in two particular types of practical applications – reflection measurements made from a platform moving with nonuniform speed or on a slightly-perturbed regular grid. Extension to 3D acquisition geometries is not impeded by any obvious obstacle.

ACKNOWLEDGMENTS

I am grateful to Jonathan Franklin and Paul Sava for the helpful discussions and to Biondo Biondi for bringing relevant references to my attention.

APPENDIX

A natural question occurs when removing a common assumption like regular sampling: Has it been discreetly incorporated into some mathematical result which may be used unknowingly?

This is why I will present a derivation of the 15° and 45° approximations of the wave equation, starting from the basic laws of mechanics. The derivation will not "open" the Laplacian in (1), keeping it as an invariant to the very end. The derivation is not original: it is based on Claerbout (1985a) and Kjartansson (1978).

The wave equation in an acoustic medium

Let x_i, where $i = 1,2,3$ be three orthogonal directions and $\vec{x}$ the position vector in a coordinate system associated with the three directions. Let us define $\rho = \rho(\vec{x})$ as the mass per volume unit in the acoustic medium, $\vec{u} = \vec{u}(\vec{x})$ as the velocity of the acoustic medium and K as the bulk modulus of the acoustic medium. The second law of dynamics states that mass $\times$ acceleration = force = - pressure gradient:

$$\rho \frac{\partial u_i}{\partial t} = -\frac{\partial P}{\partial x_i}. \tag{15}$$

Energy can be stored by compression and volume variation. If

$$\vec{u}(\vec{x} + \delta\vec{x}) \neq \vec{u}(\vec{x}), \tag{16}$$

we say that the flow diverges (the volume changes). This leads to a pressure variation, proportional to the divergence of the velocity:

$$-\frac{\partial P}{\partial t} = K\left(\frac{\partial u_1}{\partial x_1} + \frac{\partial u_2}{\partial x_2} + \frac{\partial u_3}{\partial x_3}\right). \tag{17}$$

The wave equation in an acoustic medium can be deduced from (15) and (17) as follows. Derivate (17) with respect to time:

$$\frac{\partial^2 P}{\partial t^2} = -K \sum_{i=1}^{3} \frac{\partial^2 u_i}{\partial t \partial x_i}. \tag{18}$$

Divide (15) by ρ and derivate it with respect to the axis x_i:

$$\frac{\partial^2 u_i}{\partial t \partial x_i} = -\frac{\partial}{\partial x_i}\frac{1}{\rho}\frac{\partial P}{\partial x_i}. \tag{19}$$

Plug (19) in (18):

$$\frac{\partial^2 P}{\partial t^2} = K \sum_{i=1}^{3} \frac{\partial}{\partial x_i}\frac{1}{\rho}\frac{\partial P}{\partial x_i}. \tag{20}$$

Approximation: ρ is a constant that does not depend on the position vector. By denoting the acoustic waves propagation velocity through the medium by v, where

$$v^2 = \frac{K}{\rho}, \tag{21}$$

we obtain the acoustic wave equation:

$$\frac{\partial^2 P}{\partial t^2} = v^2 \sum_{i=1}^{3} \frac{\partial^2 P}{\partial x_i^2}. \tag{22}$$

New notations and definitions

Until now the proof was pure physics. But because in seismology the depth axis is "special," we will change notations. Axis x_3 will be denoted by z, and the $\vec{x}$ will denote the surface position vector with the components (x_1, x_2). Also, the Laplacian will be the operator,

$$\Delta = \frac{\partial^2}{\partial x_1^2} + \frac{\partial^2}{\partial x_2^2}. \tag{23}$$

We will use the Fourier transform of the pressure field along the time axis:

$$P(\vec{x}, z, \omega) = F\{P(\vec{x}, z, t)\} = \int_{-\infty}^{\infty} P(\vec{x}, z, t) e^{i\omega t} dt. \tag{24}$$

The following property of the Fourier transform will be needed:

$$F\left\{\frac{\partial^2 P(\vec{x}, z, t)}{\partial t^2}\right\} = -\omega^2 P(\vec{x}, z, \omega). \tag{25}$$

The spatial frequency is defined as:

$$m(\vec{x}, z) = \frac{\omega}{v(\vec{x}, z)}. \tag{26}$$

Let $\bar{v}$ be a spatial average of v in the medium, a known constant that does not depend on $\vec{x}$ or z. We also define

$$\bar{m} = \frac{\omega}{\bar{v}} \tag{27}$$

and the function

$$Q(\vec{x}, z, \omega) = P(\vec{x}, z, \omega) e^{-i\bar{m}z}. \tag{28}$$

The index notation for derivatives will be used from now on. The symbol $\forall$ will denote the phrase "for all."

Downward continuation

Given the values of the function $P(\forall\vec{x}, z, \forall\omega)$, downward continuation consists of finding the values of $P(\forall\vec{x}, z + \delta z, \forall\omega)$. An expression describing this process lays at the end of the following proof: Obtain the Helmholtz equation by applying the Fourier transform defined by (24) to the wave equation (22) while taking into account the notation (26) and the property (25) and rearranging:

$$\Delta P + P_{zz} + m^2 P = 0. \tag{29}$$

By derivating relation (28) with respect to x and z we obtain:

$$P_{x_i} = Q_{x_i} e^{i\bar{m}z}, \tag{30}$$

$$\Delta P = (\Delta Q) e^{i\bar{m}z}, \tag{31}$$

$$P_z = (Q_z + i\bar{m} Q) e^{i\bar{m}z}, \tag{32}$$

$$P_{zz} = (Q_{zz} + 2i\bar{m} Q_z - \bar{m}^2 Q) e^{i\bar{m}z}. \tag{33}$$

By plugging into in (29) and eliminating the exponential, we get:

$$\Delta Q + Q_{zz} + 2i\bar{m} Q_z + \left(m^2 - \bar{m}^2\right) Q = 0. \tag{34}$$

The second derivative with respect to z can be eliminated by derivating with respect to z, multiplying by $\frac{i}{2\bar{m}}$, and adding the result to (34):

$$\frac{i}{2\bar{m}} Q_{zzz} + \frac{i}{2\bar{m}} (\Delta Q)_z + \Delta Q + 2i\bar{m} Q_z + \frac{i}{2\bar{m}} \left(m^2 - \bar{m}^2\right) Q_z + \left(m^2 - \bar{m}^2\right) Q + \frac{im}{\bar{m}} \frac{\partial m}{\partial z} Q = 0. \tag{35}$$

Note that no approximation has been made between the wave equation (22) and this point. Eq. 35 is simply the wave equation in a different coordinate system. Now Q_{zzz} is approximated by zero:

$$\frac{i}{2\bar{m}} (\Delta Q)_z + \Delta Q + 2i\bar{m} Q_z + \frac{i}{2\bar{m}} \left(m^2 - \bar{m}^2\right) Q_z + \left(m^2 - \bar{m}^2\right) Q + \frac{im}{\bar{m}} \frac{\partial m}{\partial z} Q = 0. \tag{36}$$

For the case of a homogenous medium, $\bar{m} = m$ and the equation turns into the familiar 45° equation:

$$\frac{i}{2\bar{m}} (\Delta Q)_z + \Delta Q + 2i\bar{m} Q_z = 0. \tag{37}$$

The 15° equation is obtained by neglecting the Q_{xxz} term also:

$$\Delta Q + 2i\bar{m} Q_z = 0. \tag{38}$$

Downward continuation proceeds by considering

$$Q(\forall \vec{x}, z, \forall \omega) = P(\forall \vec{x}, z, \forall \omega) \tag{39}$$

then by using one of the equations 36, 37 or 38 to find the values of $Q(\forall \vec{x}, z + \delta z, \forall \omega)$ and by finally finding P by undoing the variable change:

$$P(\forall \vec{x}, z + \delta z, \forall \omega) = Q(\forall \vec{x}, z + \delta z, \forall \omega) e^{im_{(\vec{x},z)} \delta z}. \tag{40}$$

REFERENCES

Aldroubi, A., and Grochenig, K., 2001, Nonuniform sampling and reconstruction in shift-invariant spaces: SIAM review, **43**, no. 4, 585–620.

Claerbout, J. F., 1985a, Fundamentals of geophysical data processing: with applications to petroleum prospecting: Blackwell Scientific Publications.

Claerbout, J. F., 1985b, Imaging the Earth's Interior: Blackwell Scientific Publications.

Claerbout, J. F. Basic Earth Imaging:. http://sepwww.stanford.edu/sep/prof/bei/toc_html, 1999.

Dellinger, J., and Muir, F., 1986, Finite differencing with uneven spatial sampling: SEP–**48**, 269–276.

Kjartansson, E., 1978, Modeling and migration with the monochromatic wave equation - variable velocity and attenuation: SEP–**15**, 1–19.

Marfurt, K. J., 1984, Accuracy of finite-difference and finite-element modeling of the scalar and elastic wave equations: Geophysics, **49**, no. 5, 533–549.